Origins of tropospheric ozone interannual variation over Réunion: A model investigation

Junhua A Liu, Jose A Rodriguez, Anne A Thompson, Jennifer A Logan, Anne D Douglass, Mark A Olsen, Stephen D Steenrod, Françoise Posny

AGU PUBLICATIONS

JGR

Journal of Geophysical Research: Atmospheres

RESEARCH ARTICLE
10.1002/2015JD023981

Origins of tropospheric ozone interannual variation over Réunion: A model investigation

Junhua Liu[1,2], Jose M. Rodriguez[2], Anne M. Thompson[2], Jennifer A. Logan[3], Anne R. Douglass[2], Mark A. Olsen[2,4], Stephen D. Steenrod[1,2], and Françoise Posny[5]

[1]Universities Space Research Association, GESTAR, Columbia, Maryland, USA, [2]NASA Goddard Space Flight Center, Greenbelt, Maryland, USA, [3]School of Engineering and Applied Sciences, Harvard University, Cambridge, Massachusetts, USA, [4]Goddard Earth Science, Technology and Research Center, Morgan State University, Baltimore, Maryland, USA, [5]Laboratoire de l'Atmosphère et des Cyclones, Université de La Réunion/CNRS, Réunion, France

Abstract Observations from long-term ozonesonde measurements show robust variations and trends in the evolution of ozone in the middle and upper troposphere over Réunion Island (21.1°S, 55.5°E) in June–August. Here we examine possible causes of the observed ozone variation at Réunion Island using hindcast simulations by the stratosphere-troposphere Global Modeling Initiative chemical transport model for 1992–2014, driven by assimilated Modern-Era Retrospective Analysis for Research and Applications meteorological fields. Réunion Island is at the edge of the subtropical jet, a region of strong stratospheric-tropospheric exchange. Our analysis implies that the large interannual variation (IAV) of upper tropospheric ozone over Réunion is driven by the large IAV of the stratospheric influence. The IAV of the large-scale, quasi-horizontal wind patterns also contributes to the IAV of ozone in the upper troposphere. Comparison to a simulation with constant emissions indicates that increasing emissions do not lead to the maximum trend in the middle and upper troposphere over Réunion during austral winter implied by the sonde data. The effects of increasing emission over southern Africa are limited to the lower troposphere near the surface in August–September.

Key Points:
- The GMI-CTM Model simulated the main features of the observed ozone IAV over Réunion
- Stratospheric input plays an important role in the tropospheric ozone IAV over Réunion
- Changes in emissions have little influence on middle and upper tropospheric ozone over Réunion

Supporting Information:
- Figure S1 caption
- Figure S1

Correspondence to:
J. Liu,
junhua.liu@nasa.gov

Citation:
Liu, J., J. M. Rodriguez, A. M. Thompson, J. A. Logan, A. R. Douglass, M. A. Olsen, S. D. Steenrod, and F. Posny (2016), Origins of tropospheric ozone interannual variation over Réunion: A model investigation, *J. Geophys. Res. Atmos.*, *121*, 521–537, doi:10.1002/2015JD023981.

Received 23 JUL 2015
Accepted 7 DEC 2015
Accepted article online 12 DEC 2015
Published online 8 JAN 2016

1. Introduction

Tropospheric ozone plays an important role in the oxidative capacity of the troposphere and in atmospheric radiative forcing [e.g., *Lacis et al*., 1990; *Fiore et al*., 2002; *Forster et al*., 2007; *Sitch et al*., 2007; *Stevenson et al*., 2013]. It acts as a direct greenhouse gas in the upper troposphere and lower stratosphere and has contributed significantly to climate change. It also impacts the air quality near the surface, with harmful effects on human health and crop yields [e.g., *Bell et al*., 2005; *Silva et al*., 2013]. Ozone is produced in the troposphere by photochemical oxidation of CO and volatile organic compounds in the presence of nitrogen oxides (NO_X) [e.g., *Logan et al*., 1981]. These ozone precursors are emitted both from anthropogenic sources, including fossil fuel combustion and biomass burning, and from natural sources such as lightning. Moreover, in regions of subsidence, tropospheric ozone may be significantly affected by ozone input from the stratosphere. Long-range transport, most significant in the middle and upper troposphere where the ozone lifetime is several weeks [*Fusco and Logan*, 2003], also contributes to the tropospheric ozone distribution [*Sudo and Akimoto*, 2007].

A recent study by *Thompson et al*. [2014] identified a significant increase in tropospheric ozone at Réunion (21°S, 55°E) in June-July-August (JJA) from 1992 to 2011 based on ozonesonde measurements. The observed increase is up to 50%/decade in the upper troposphere. This result extended the study by *Clain et al*. [2009], who found a strong positive ozone trend in the middle and upper troposphere in JJA based on Réunion sonde for 1992 to 2008. The sonde data also show large interannual variability (IAV), which complicates the estimation and diagnosis of trends. In this study, we use the stratosphere-troposphere Global Modeling Initiative chemical transport model (GMI-CTM) model to interpret the observed IAV and trends of tropospheric ozone over Réunion from 1992 to the present. In so doing, we investigate the impact of stratospheric input and surface emissions during the past 20 years.

Earlier studies have used tropospheric CTMs to examine the response of tropospheric ozone to changes in stratospheric input and in surface emissions; these models used a simple treatment of stratospheric influence, in which they either used the synthetic ozone approach developed by *McLinden et al*. [2000] of

specifying the flux (e.g., the Goddard Earth Observing System (GEOS)-Chem model in *Fusco and Logan* [2003] and *Hess and Zbinden* [2013]) or specified ozone in the lower stratosphere (e.g., *Karlsdottir et al*. [2000] and the Goddard Institute for Space Studies model in *Fusco and Logan* [2003]). *Pozzoli et al*. [2011] simulated tropospheric composition for 1980–2005 using an aerosol-chemistry climate model driven by the European Centre for Medium-Range Weather Forecasts 40 year reanalysis (ERA-40) data and operational analyses. The two simulations with constant and varying anthropogenic emissions show similar IAV in surface ozone, suggesting that changes in meteorology and natural emissions contribute greatly to the ozone IAV, which may mask contrasting regional trends driven by anthropogenic emissions in surface ozone in any given period. *Lin et al*. [2014] argued that shifts in atmospheric circulation patterns contribute to the observed tropospheric ozone trends at Mauna Loa, the western U.S., and the northern midlatitudes in recent decades based on a suite of chemistry-climate model simulations. *Hess et al*. [2015] analyzed the effects of stratospheric input to tropospheric ozone variations over the Northern Hemisphere midlatitudes with four ensemble simulations of the free-running Whole Atmosphere Community Climate Model for 1953 to 2005. Their model used a standard stratospheric chemical mechanism, but with simple CH_4-NO_X chemistry in the troposphere with constant surface chemical emissions. The agreement of the simulated and observed tropospheric ozone IAV in *Hess et al*. [2015] suggests that natural variability plays a big role controlling the IAV of tropospheric ozone over the Northern Hemisphere. Most of these studies focused on the northern hemispheric extratropics. Far fewer studies have focused on the long-term behavior of ozone in Southern Hemisphere owing to a lack of suitable observations.

In our study, taking advantage of the multiyear record from Réunion sonde and hindcast simulations from the GMI-CTM model [*Duncan et al*., 2007; *Strahan et al*., 2007], we investigate the causes of observed interannual and decadal variations of tropospheric ozone over Réunion. Our analysis is based on a series of hindcast simulations for 1992–2014 with the GMI-CTM driven by assimilated Modern-Era Retrospective Analysis for Research and Applications (MERRA) meteorological fields [*Rienecker et al*., 2011]; the GMI-CTM includes a comprehensive stratospheric and tropospheric chemical mechanism. The simulations include a stratospheric ozone tracer to examine the stratospheric contribution. We also use a control simulation with constant emissions to explore the influence from surface emissions.

Réunion Island (20.8°S, 55.5°E) is in the western part of the South Indian Ocean, about 1000 km east of Madagascar. In the upper troposphere, the position of Réunion is near the boundary between tropical air with low ozone and the subtropical jet region with high ozone [*Thompson et al*., 2014, Figure 1]. The dominant meteorological features in the troposphere over Réunion are subject to competition between tropical and subtropical influences on the general circulation. The meteorology is also affected by the perturbations from the South Indian Ocean anticyclone and wave propagation in the westerlies [*Waugh and Polvani*, 2000; *Randriambelo et al*., 2003]. Observations and meteorological data show that tropospheric ozone variations over this region are mainly influenced by stratospheric intrusions through various dynamical mechanisms [*Baray et al*., 1998; *Postel and Hitchman*, 1999; *Baray et al*., 2003; *De Bellevue et al*., 2007; *Clain et al*., 2009]. *Skerlak et al*. [2014] extracted a global climatology of stratosphere-troposphere exchange (STE) using the ERA-Interim data set from 1979 to 2011. Their results show a large latitudinal gradient in the ozone flux from stratosphere to troposphere to the south of Réunion in JJA as well as other seasons. Tropospheric ozone at Réunion shows a strong seasonal cycle with an austral winter-spring maximum and summer minimum [*Baldy et al*., 1996; *Taupin et al*., 1999; *Randriambelo et al*., 2000]. The summer minimum is due to a combination of photochemical loss and inflow of tropical marine air with the development of deep convection [*Taupin et al*., 1999; *Clain et al*., 2009]. The winter-spring maximum has been attributed by several previous studies to a combined influence of surface emission and stratospheric influence [e.g., *Taupin et al*., 1999; *Randriambelo et al*., 2000; *Thompson et al*., 1996, 2003].

Réunion is located downwind of emissions from southern Africa and Madagascar. Several studies based on trajectory statistics suggested that a portion of African emissions might be transported to the Indian Ocean [*Garstang et al*., 1996; *Piketh et al*., 2002; *Sudo and Akimoto*, 2007; *Thompson et al*., 2014]. Southern Africa, one of the major biomass burning regions in the Southern Hemisphere, also has an abundance of industrial and other anthropogenic sources. *Lelieveld et al*. [2004] found that anthropogenic NO_X emissions doubled from 1977 to 2001 (0.8 to 1.6 Tg/yr) over Africa based on a historical emission inventory. *Sauvage et al*. [2007] showed that emissions over the eastern regions (India, Southeast Asia, and Australia) have a broad influence throughout the Pacific and Indian Oceans, with the maximum contribution for ozone

changes over Réunion region in JJA. They argued that the eastern source emissions were transported to the upper level anticyclone associated with the Indian monsoon system [*Hoskins and Rodwell*, 1995; *Rodwell and Hoskins*, 2001], then trapped in the Tropical Easterly Jet, which peaks in JJA [*Hastenrath and Wu*, 1982], and transported cross equator to North Africa, the Atlantic, and Indian Ocean. The changes in anthropogenic emissions from the eastern region may also contribute to the observed positive trends at Réunion. We will examine the effects of changes of emissions using a sensitivity simulation with constant emissions, including emissions from biomass burning, fossil fuel, and biofuel burning, in section 3.3.

Section 2 provides an overview of the GMI-CTM simulations and the ozonesonde measurements. Section 3.1 evaluates the vertical and spatial distribution of tropospheric ozone in the model using ozonesonde data and Global Modeling and Assimilation Office (GMAO) assimilated data. Section 3.2 presents a diagnostic study of factors controlling the observed ozone IAV in the upper troposphere at Réunion using GMI-CTM model simulations. Section 3.3 focuses on the trends in observed and model simulated tropospheric ozone. Conclusions and the discussion of the dynamical effects on tropospheric ozone IAV are described in section 4.

2. Measurements and Model

2.1. GMI CTM Hindcast Simulations

We used the GMI CTM [*Duncan et al*., 2007; *Strahan et al*., 2007] driven by MERRA reanalysis meteorology [*Rienecker et al*., 2011] (http://gmao.gsfc.nasa.gov/research/merra/). MERRA was produced with the NASA Goddard Earth Observing System (GEOS) version 5.2.0 data assimilation system with the native horizontal resolution of 0.67° × 0.5° and 72 vertical levels. The vertical resolution of MERRA fields is ~1 km in the upper troposphere and lower stratosphere. We regrid to 2° × 2.5° for input to the base GMI-CTM simulations. MERRA uses a modified version of the Relaxed Arakawa-Schubert convective scheme described by *Moorthi and Suarez* [1992]. The model reads in the planetary boundary layer (PBL) from MERRA and follows the full mixing scheme where emissions and concentrations of individual species are evenly distributed in the PBL. The model includes a complete treatment of stratospheric and tropospheric chemistry coupled with aerosol mechanism derived from the Global Ozone Chemistry Aerosol Radiation and Transport (GOCART) model [*Chin et al*., 2002]. Biogenic emissions of isoprene and monoterpenes follow the latest version of the Model of Emissions of Gases and Aerosols from Nature (MEGAN) algorithm [*Guenther et al*., 2006]. Biomass burning emissions are from the Global Fire Emission Database, GFED3 [*van der Werf et al*., 2010]. Emission before 1997 are retrieved from GFED3 emission climatology averaged for 2001 to 2009 with regional-scale IAV applied, which was derived from satellite information on fire activity (Along Track Scanning Radiometer) and/or aerosol optical depths from the Total Ozone Mapping Spectrometer (TOMS) by *Duncan et al*. [2003]. Anthropogenic emissions are based on the Emission Database for Global Atmospheric Research 3.2 inventory [*Olivier et al*., 2005], overwritten with the regional inventories for North America, Europe, and Asia. More details are given in *Strode et al*. [2015]. Emission data were only available through year 2011 when our hindcast simulations were conducted. Consequently, we repeat the emissions of year 2011 for years 2012–2014. The lightning NO_X is calculated online following the scheme described by *Allen et al*. [2010]. The global total of NO_x from lightning is set the same of 5.00 Tg N/yr every year in the hindcast. Methane mixing ratios are specified in the two lowest model levels, using time-dependent zonal means from NOAA/Global Monitoring Division (GMD). Other long-lived source gases important in the stratosphere, such as N_2O, CFCs, and halocarbons, are forced monthly at the two lowest model levels based on the A2 scenario as described in *Strahan et al*. [2007]. Stratospheric aerosol distributions/trends are from International Global Atmospheric Chemisty/Stratospheric Processes and their Role in Climate and have IAV [*Stolarski et al*., 2006].

Our standard simulation (labeled as Hindcast-VE) used in this study for 1992–2014 includes monthly and interannually varying emissions of fossil fuel, biomass burning, and biofuel. We carry out a control run with constant emissions fixed at year 2000 levels, which is labeled as Hindcast-CE. We also conduct a high-resolution simulation (labeled as Hindcast-VE-HR) at 1.25° × 1° horizontal resolution to explore the effect of model's horizontal resolution on ozone simulation.

The model includes a stratospheric ozone tracer ($StratO_3$). The $StratO_3$ is defined relative to a dynamically varying tropopause tracer (e90) [*Prather et al*., 2011], which has been implemented in the GMI model. The e90 tracer is an artificial tracer emitted at the surface uniformly (100 ppb) with a 90 day *e*-folding lifetime. In our simulation, the e90 tropopause value is 90 ppb. The $StratO_3$ tracer is set equal to ozone in

the stratosphere and is removed in the troposphere with the loss frequency (chemistry and deposition) archived from daily output of Hindcast-VE simulation in this study. The simple $O_X - HO_X$ cycle ($O(^1D) + H_2O -> 2\ OH$; $HO_2 + O_3 -> 2\ O_2 + OH$; $OH + O_3 -> HO_2 + O_2$) is applied to determine destruction of odd oxygen. There is no production of $StratO_3$ in the troposphere. Using the $StratO_3$ tracer allows quantification of ozone of stratospheric origin in the troposphere at a given location and time. This approach has also been adopted in the high-resolution Geophysical Fluid Dynamics Laboratory Atmospheric Model 3 [*Lin et al*., 2012].

2.2. Réunion Ozone Sonde Measurements

Vertical ozone profiles were measured since September 1992 at Réunion Island from radiosondes using three manufacturers (Science Pump Corporation: SPC, EN-SCI Corporation: ENSCI-Z, and ENSCI-Droplet Measurement Technologies: ENSCI-DMT) [*Baldy et al*., 1996; *Baray et al*., 2006; *Thompson et al*., 2014]. Although these changes are not recorded in the Southern Hemisphere Additional Ozonesondes (SHADOZ) metadata (http://croc.gsfc.nasa.gov/shadoz/), the lacking of instrument uniformity could have minor impacts on calculated trends. Overall, sonde data quality assurance during SHADOZ's period (1998–2014) can be inferred from comparisons between sonde total ozone at Réunion and TOMS (to 2005) and Ozone Monitoring Instrument (OMI) (after 2005) overpass, as well as Systéme d'Analyse par Observation Zénitale (SAOZ) [*Thompson et al*., 2003, 2007, 2012], which do not show evidence of systematic instrumental change. The ozone measurements are on a biweekly/monthly basis. A standard meteorological radiosonde is attached to the ozonesondes to simultaneously transmit the profiles of atmospheric temperature, pressure, and humidity, along with the ozone data: Vaisala RS80 (prior to September 2007) then Modem M2K2 and M10 (since April 2013). The Modem sondes measure in addition the position, the wind speed, and the direction (Doppler GPS). *Thompson et al*. [2012] showed that the column ozone over Réunion for 2005–2009 as measured by the sondes was within 2–3% of OMI satellite measurements and the measurements of SAOZ instrument, colocated at Réunion Island.

To compare GMI-CTM model output with the Réunion sonde profiles, we extract the model grid box containing Réunion Island and sample the model profiles on the date of each observation. The Réunion ozonesondes provide high vertical resolution profiles of ozone (~100 m) through the depth of the troposphere. We convert the sonde profiles from high-resolution to the low-resolution vertical grid used in model. In our algorithm, we integrate the high-resolution sonde profiles at their pressure levels to get the accumulated partial column ozone profiles in Dobson units (DU). We then interpolate the integrated profiles into the MERRA reduced vertical grid with 47 fixed pressure levels and convert them back to mixing ratio in ppbv following the method as described in *Ziemke et al*. [2001].

2.3. GMAO Assimilated Ozone Data

We also used assimilated tropospheric ozone to evaluate the overall model performance. This assimilated data set is produced by ingesting OMI v8.5 total column ozone and Microwave Limb Sounder (MLS) v3.3 ozone profiles into a version of the Goddard Earth Observing System, version 5 (GEOS-5) data assimilation system [*Rienecker et al*., 2011]. No ozonesonde data are used in the assimilation. *Wargan et al*. [2015] provide details of the GEOS-5.7.2 assimilation system, which for this application is run with a horizontal resolution of 2° latitude by 2.5° longitude and with 72 vertical layers between the surface and 0.01 hPa. For the troposphere, the assimilation applies only a dry deposition mechanism at the surface without any chemical production or loss. This algorithm works since the ozone lifetime is much longer than the 6 h analysis time steps. *Ziemke et al*. [2014] evaluated the tropospheric ozone profiles derived from OMI and MLS measurements using three strategies to quantify the tropospheric ozone column (this GEOS-5 assimilation, trajectory mapping, and direct profile retrieval using the residual method) with ozonesonde observations and GMI model simulations. They found that the tropospheric ozone product from the GEOS-5 assimilation is the most realistic one. *Wargan et al*. [2015] also demonstrate that the upper tropospheric ozone (500 hPa to the tropopause) from GEOS-5 assimilation is in good agreement with independent observations from ozonesondes. Therefore, we treat the ozone from the GEOS-5 assimilation as a reference value and use it to evaluate our GMI model simulation. We use partial column ozone integrated from 500 hPa to the tropopause from the GEOS-5 assimilation, because there is no direct observational constraint in the analysis in the lower troposphere (the OMI kernels have no weight in the lowest layers) and the assimilation system does not account for chemical production by fast chemical processes, such as NO_X emissions [*Wargan et al*., 2015]. We use the

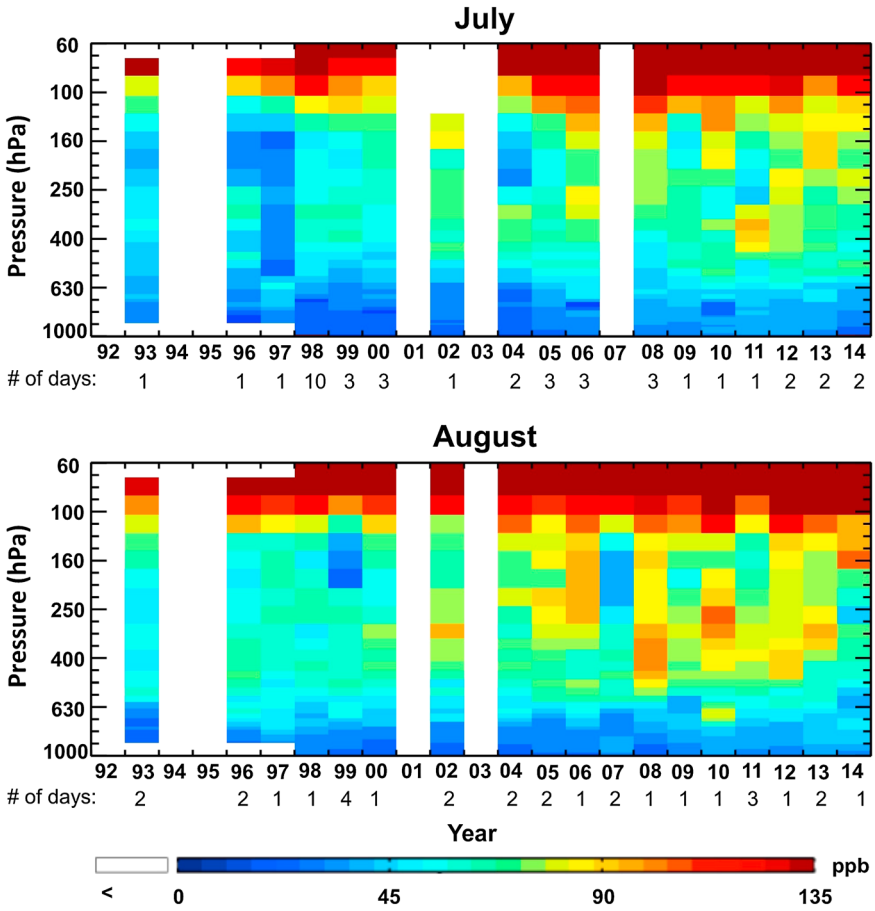

Figure 1. Temporal evolution of ozone profiles from Réunion ozonesonde in July and August from 1992 to 2014. High-resolution Réunion sonde profiles are integrated to MERRA reduced vertical grid (47 fixed pressure levels).

same tropopause as defined by the lowest of the 3.5 potential vorticity unit/380 K control surface to calculate the tropospheric ozone column.

3. Results

3.1. Ozone Profile and Model Evaluation

The temporal evolution of observed ozone vertical profiles from Réunion ozonesonde in July and August from 1992 to 2014 is shown in Figure 1. The ozone concentration in the middle and upper troposphere stayed low in the early 1990s then increased continuously around year 2000 in both July and August. The profiles in the 1990s have steep ozone gradients in the upper troposphere and lower stratosphere and a relatively uniform and low ozone layer in the middle and lower troposphere. The profiles in the 2000s show greater IAV and occasionally have large increases of ozone in the middle and upper troposphere (e.g., July 2006 and 2011 and August 2006, 2008, 2010, and 2013). Evidently, the occurrence of these ozone maxima in the 2000s is the main reason for the positive ozone trends in July and August calculated by *Thompson et al.* [2014] over Réunion.

A recent study by *Lin et al.* [2015] concluded that the weekly ozone sonde measurements at Trinidad Head and Boulder do not faithfully capture the actual variability of mean midtropospheric ozone due to the sparse sample frequency. The issue of the sampling frequency of sondes (weekly or sparser at many sites) has also been raised by many previous studies, often in the context of tropospheric trends [e.g., *Cooper et al.*, 2010; *Logan et al.*, 2012], but also in terms of climatology [*Logan*, 1999], and in terms of different types of variability, including interannual [e.g., *Logan et al.*, 2012; *Saunois et al.*, 2012]. We therefore used model simulations to check the adequacy of the sampling frequency over Réunion. Figure 2 compares simulated monthly mean

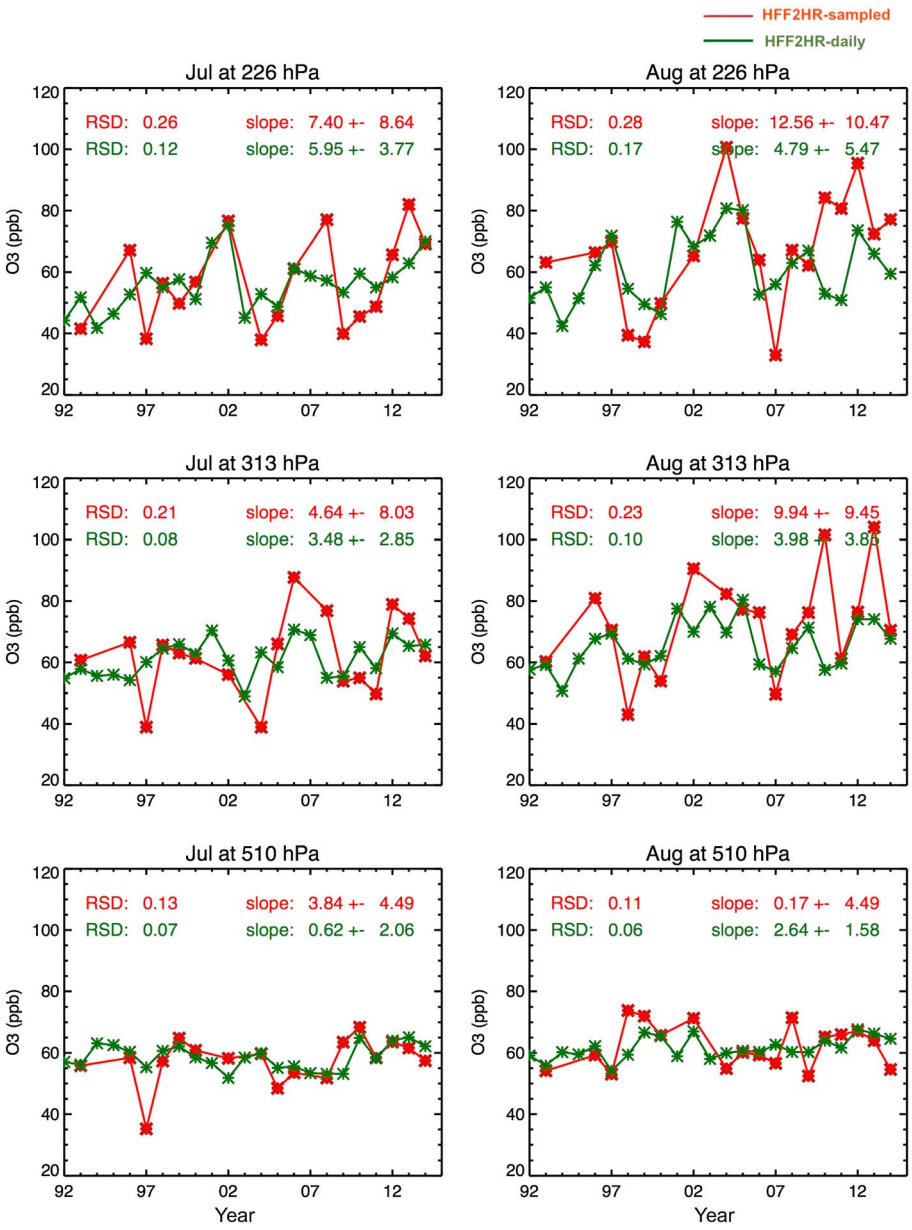

Figure 2. Comparison of simulated monthly mean ozone mixing ratio averaged from the GMI-CTM Hindcast-VE-HR run (1 × 1.25, with varying emissions) cosampled with the available sonde observations (red), and the mean determined from daily ozone fields archived from the model (green) for July and August from 1992 to 2014 at 226 hPa, 313 hPa, and 510 hPa. RSD in each panel is the relative standard deviation, which represents the coefficient of variation of each line. The slope in each panel represents the calculated linear trends at the 90% confidence level with unit ppb/decade. Both RSD and slope follow the same color scheme as the lines.

ozone mixing ratio at 226 hPa, 313 hPa, and 510 hPa averaged from the GMI-CTM Hindcast-VE-HR run (1° × 1.25°, with varying emissions) cosampled with the available sonde observations (red lines) and the monthly mean of the model daily output (green lines) from 1992 to 2014. The phases of interannual variations are often similar between the two monthly means, with some obvious discrepancies particularly in the upper troposphere. We show the relative standard deviations to quantify the interannual variations of the simulated ozone mean with the two sampling methods. The variations in the cosampled means tend to have a larger magnitude. This is not unexpected, as Réunion is located in a both dynamically and chemically active region with a large ozone gradient, and the sampling is infrequent. The agreement of monthly

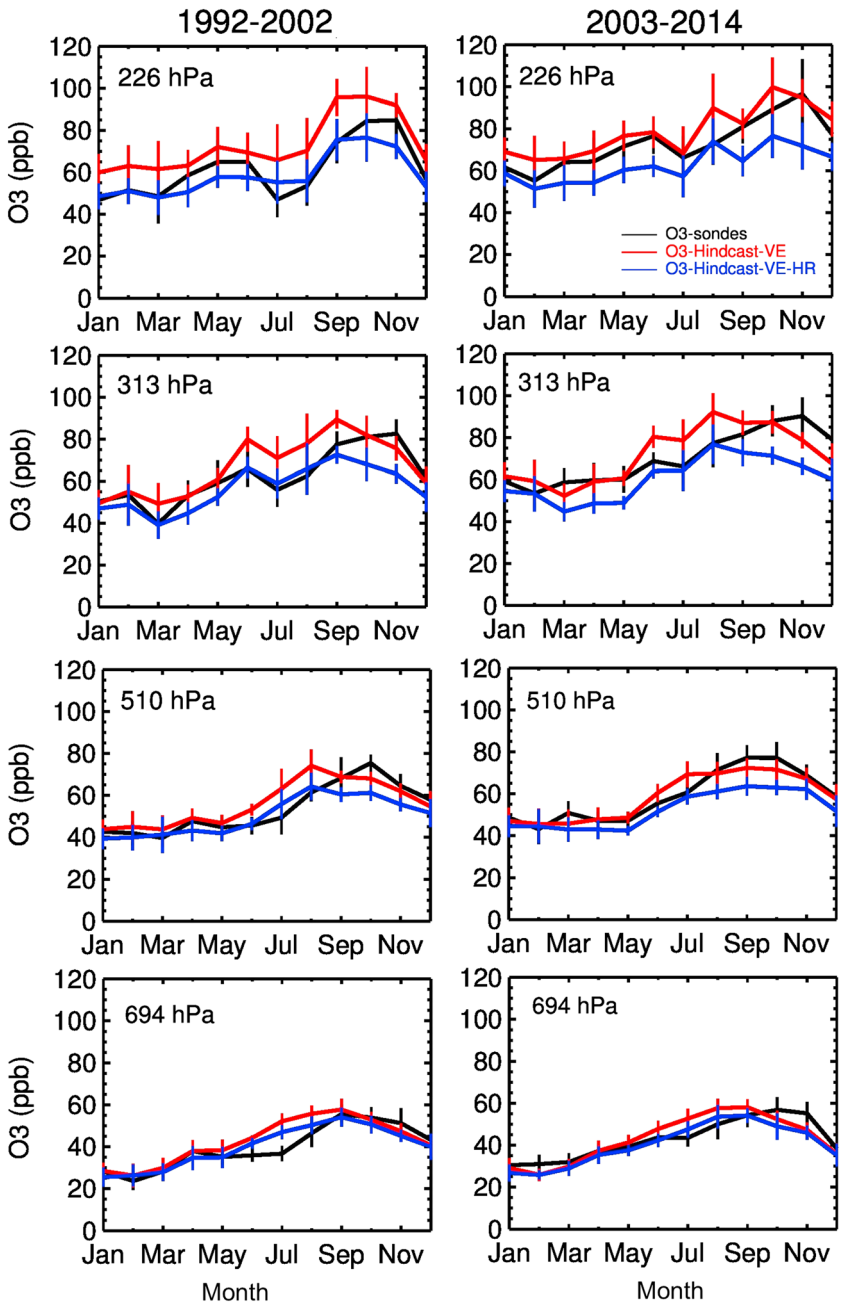

Figure 3. Comparison of GMI-CTM Hindcast-VE (2 × 2.5, red lines), Hindcast-VE-HR (1 × 1.25, blue lines), and observed (black lines) monthly mean averaged over (left column) 1992 to 2002 and (right column) 2003 to 2014 at 226 hPa, 313 hPa, 510 hPa, and 694 hPa. Vertical bars indicate ±2 standard error of the monthly mean values. The model results are sampled on the date of sonde measurements. High-resolution Réunion sonde profiles are integrated to MERRA reduced vertical grid (47 fixed pressure levels).

means between these two sampling methods is better at 510 hPa than at upper levels. We also compare the monthly mean from daily output and the means determined with different sampling frequencies (e.g., monthly, biweekly, and weekly). The results suggest that increasing sampling frequency to four per month would be enough to reproduce the IAV of the mean from daily output. Although the current sparse sampling cannot fully reproduce the IAV in the monthly means of daily output in the upper troposphere, we can evaluate how well the model captures the variability that is revealed by the sonde data by cosampling the model on the dates of the soundings and then use the model to examine mechanisms influencing the IAV.

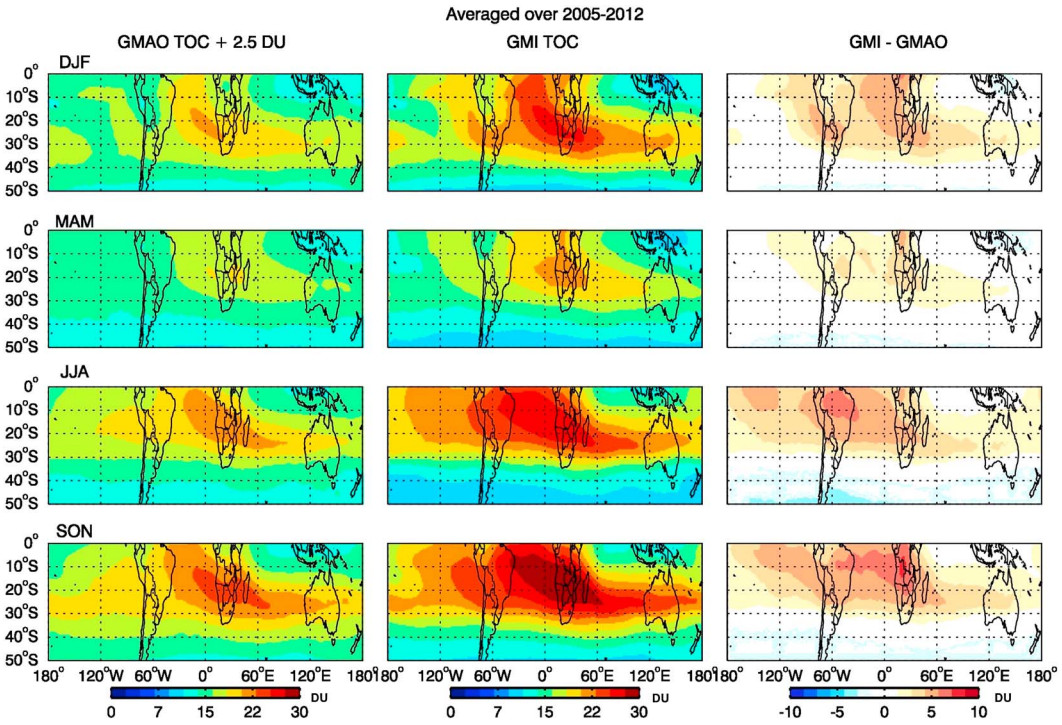

Figure 4. Seasonal maps of tropospheric partial column ozone (in Dobson units, integrated from 500 hPa to the tropopause) for December–February (DJF), March–May (MAM), June–August (JJA), and September–November (SON) seasons averaged from 2005 to 2012 for (left column) GMAO assimilated ozone and (middle column) GMI-CTM Hindcast-VE ozone and (right column) their absolute difference. The GMAO assimilated ozone has been adjusted by adding 2.5 DU based on *Wargan et al.* [2015].

Unlike the IAV, the derived trends are very sensitive to the sampling frequency, as well as other factors, such as years used in the trend calculation (see below). In July, the mean of daily output shows statistically significant positive trends both at 226 hPa and 313 hPa. These trends become insignificant when sampled at the ozonesonde measurement time. In August, the significant positive trends in sampled monthly mean become insignificant in the monthly mean ozone of daily output at 226 hPa and 313 hPa. Given the limitations of the sampling as well as other factors affecting calculated trends, we have not focused on the trends at Reunion, except for an analysis of the influence of trends in emissions.

Figure 3 compares the modeled and observed tropospheric ozone at Réunion averaged over 1992–2002 and 2003–2014 from the upper to the lower troposphere. The observed monthly mean ozone is generally higher (~10–20 ppb) in the upper troposphere during the most recent period compared to the previous period. The difference between these two periods is smaller in both model simulations. At 226 hPa, the Hindcast-VE simulation (red) agrees very well with the observed phase of the annual cycles during both periods but is too high by 10–15 ppb for 1992–2002. From 313 hPa to 694 hPa, the Hindcast-VE simulations overestimate the observations from June to August over both periods. The overestimates are largest (~12 ppb) in the upper troposphere and decrease to ~5 ppb in the middle and lower troposphere. Ozone from the high-resolution simulation (blue) is systematically lower than that from the low-resolution simulation by an average of 15 ppb in the upper troposphere and less than 5 ppb in the lower troposphere, resulting in a better agreement with observations in June to August from 313 hPa to 694 hPa. At 226 hPa, the high-resolution simulation reduces the overestimate as seen in the low-resolution simulation for 1992–2002 but underestimates the observations for 2003–2014.

Figure 4 shows the spatial pattern of southern hemispheric ozone partial columns in the upper troposphere (integrated from 500 hPa to the tropopause) averaged over 2005 to 2012, when GMAO assimilated data are available, for the four seasons from the GMAO assimilated data set based on OMI/MLS (left column) and the GMI hindcast-VE simulation (middle column) and their absolute difference (right column). *Wargan et al.* [2015]

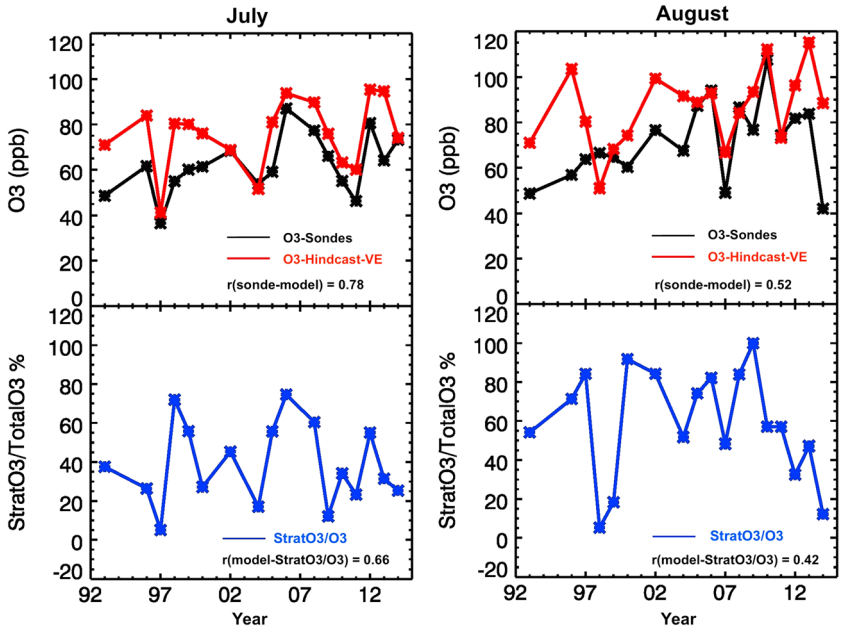

Figure 5. Time series of observed (black) and GMI-CTM Hindcast-VE simulated (red) ozone mixing ratios and the $StratO_3/O_3$ ratio (blue) at 313 hPa in (left column) July and (right column) August from 1992 to 2014. The model results are sampled on the date of sonde measurements.

argue that the UT ozone column (from 500 hPa to the tropopause) within 30°S–30°N latitude bands has a low bias of 2.5 ± 3.8 DU compared to sonde measurement. We therefore adjusted the GMAO assimilated ozone by adding 2.5 DU to compare to the GMI hindcast simulation. Both show the wave one ozone maximum, a predominantly Southern Hemisphere phenomena, with ozone maximum localized in the southern Atlantic-southern Africa-western Indian Ocean region [*Logan and Kirchhoff*, 1986; *Thompson et al*., 1996, 2003; *Sauvage et al*., 2006, 2007]. Over these ozone maximum regions, although the GMI hindcast simulations are too high compared to the assimilated ozone, most of the model overestimations are within the bias range as suggested by *Wargan et al.* [2015]. In general, the GMI hindcast simulation reproduces the seasonality and spatial distribution of the upper tropospheric column ozone from the assimilated product.

3.2. IAV

Figure 5 shows the temporal variation of observed (black) and simulated ozone (red) and the simulated $StratO_3/O_3$ ratio (blue) at 313 hPa in July and August from 1992 to 2014. The monthly mean simulations are calculated from daily output sampled on the date of sonde measurements. In July, sonde and model agree well on the IAV of O_3 at 313 hPa ($r = 0.78$, $P < 0.001$) and are similar to the phase of the IAV of the $StratO_3/O_3$ ratio. For example, both sonde and model show an ozone minimum in 1997, 2004, and 2011 when the stratospheric ozone contribution inferred from the $StratO_3/O_3$ ratio reaches a minimum. In July 1998, 2006, and 2012, both sonde and model show an ozone maximum, concurrent with the maximum in the $StratO_3/O_3$ ratio. In August, a similar but somewhat weaker coupling is observed between ozone mixing ratio and $StratO_3/O_3$ ratio at 313 hPa. The IAVs of both the simulated ozone and $StratO_3/O_3$ ratio are relatively constant through the two decades, while the IAV in observed ozone is relatively small during the first decade compared to that in the second decade (Figure 5). Therefore, the IAV of simulated ozone shows a better agreement with the IAV of sonde observations in the 2000s. An independent initial analysis of total column ozone based on satellite and a MERRA-forced GMI-CTM simulation also suggests better agreements after year 2000 (L. D. Oman, personal communication, 2015), when many more higher-resolution meteorological observations are included in the MERRA assimilation [*Rienecker et al*., 2011]. Nevertheless, the model captures many of the observed peaks and troughs in the sonde measurements. The good agreement between tropospheric ozone IAV with that of $StratO_3/O_3$ ratio during austral winter indicates that changes in the stratospheric ozone contribution play an important role in the observed IAV in winter over Réunion at 313 hPa, particularly in July when $StratO_3$ explains about 44% of the model variance.

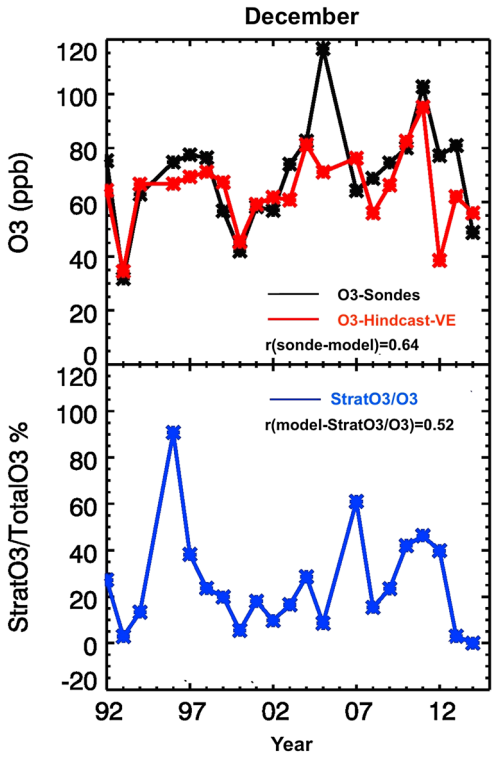

Figure 6. Time series of observed (black) and GMI-CTM Hindcast-VE simulated (red) ozone mixing ratios and the $StratO_3/O_3$ ratio (blue) at 313 hPa in December from 1992 to 2014. The model results are sampled on the date of sonde measurements.

Figure 6 shows a similar plot in December, when both STE and surface emissions over southern Africa reach their seasonal minimum. The model agrees well with the observed ozone from sondes in the upper troposphere ($r = 0.64$, $P < 0.005$). It matches the magnitudes and phase changes of observed IAV, except for 2005, 2012, and 2013. The stratospheric ozone contribution explains about ~27% of the variance of model ozone, which indicates that even in austral summer, the IAV of stratospheric input contributes to IAV of upper tropospheric ozone over Réunion.

To diagnose and examine the impact of stratospheric input and other dynamical mechanisms on the tropospheric ozone at the interannual time scale, we selected July 1997 and 2006 as two extreme examples. Figures 7a and 7b show the spatial maps of simulated ozone mixing ratio at 313 hPa in July 1997 and 2006. Both years show a similar ozone spatial pattern. Ozone reaches a minimum over Indonesia, which is caused by strong convection over this region [e.g., *Logan et al*., 2008]. The very high ozone is widespread across the southern Atlantic, southern Africa, southern Indian Ocean region, and western Pacific, centered at 30°S where the subtropical jet is located. The black star denotes the location of Réunion, with steep gradients in ozone. It is clearly seen from Figure 7 that in July 1997, Réunion is located at the edge of the ozone maximum zone, while in July 2006, Réunion is in its center. The difference in ozone over Réunion at 313 hPa is up to 20 ppb (~30%) between these two years. Figures 7c and 7d show the spatial maps of the corresponding $StratO_3/O_3$ ratio, which represent the influence of stratospheric air on tropospheric ozone. The stratospheric influence shows a minimum over the tropics and maximum contribution over the subtropics, which is closely related to the Brewer Dobson circulation [*Brewer*, 1949; *Dobson*, 1956; *Holton et al*., 1995]. Réunion is located right on the boundary of the tropical convection regions and the subtropical jet system with a sharp gradient in the stratospheric input. In July 1997, the equatorward boundary of regions with strong stratospheric influence moves southward and Réunion falls out of this region. In July 2006 Réunion falls in the region with strong stratospheric influence, resulting in the ozone maximum. Evidently, the large interannual differences in the stratospheric contribution of ozone cause the strong IAV of tropospheric ozone over Réunion. Ozone is most abundant over the regions where stratospheric influences are highest.

Figure 8 shows the profiles of observed (black) and the simulated ozone from GMI-CTM Hindcast-VE (red) and GMI-CTM Hindcast-VE-HR (blue) in July 1997 and 2006 at Réunion. In July 1997, ozone concentrations are low (~30 ppb) through the troposphere and are representative of major influence from tropical marine air. In July 2006, the ozone concentration slowly increases with altitude, with an ozone peak up to 90 ppb in the upper troposphere both in measurements and model simulations, reflecting the contributions from stratospheric high ozone air. Ozone profiles from both simulations reproduce the shape of observed ozone profile in July 1997, but the models are too high in the middle and upper troposphere by ~10 ppb. In July 2006, the ozone profile from high-resolution simulation agrees very well with the observed ozone profile below 300 hPa, while results from the low-resolution run are too high.

We also examined the influence of the prevailing horizontal transport on the IAV of tropospheric ozone near Réunion. Figure 9 shows the monthly mean ozone mixing ratio superimposed on the spatial wind pattern at 313 hPa in July 1997 and 2006. In July 1997, northwesterly winds prevail over Réunion Island and bring in tropical low ozone air. In July 2006, the southerly winds encroach from the south and converge near Réunion Island, which bring in midlatitude high ozone air, with the strongest $StratO_3$ contribution

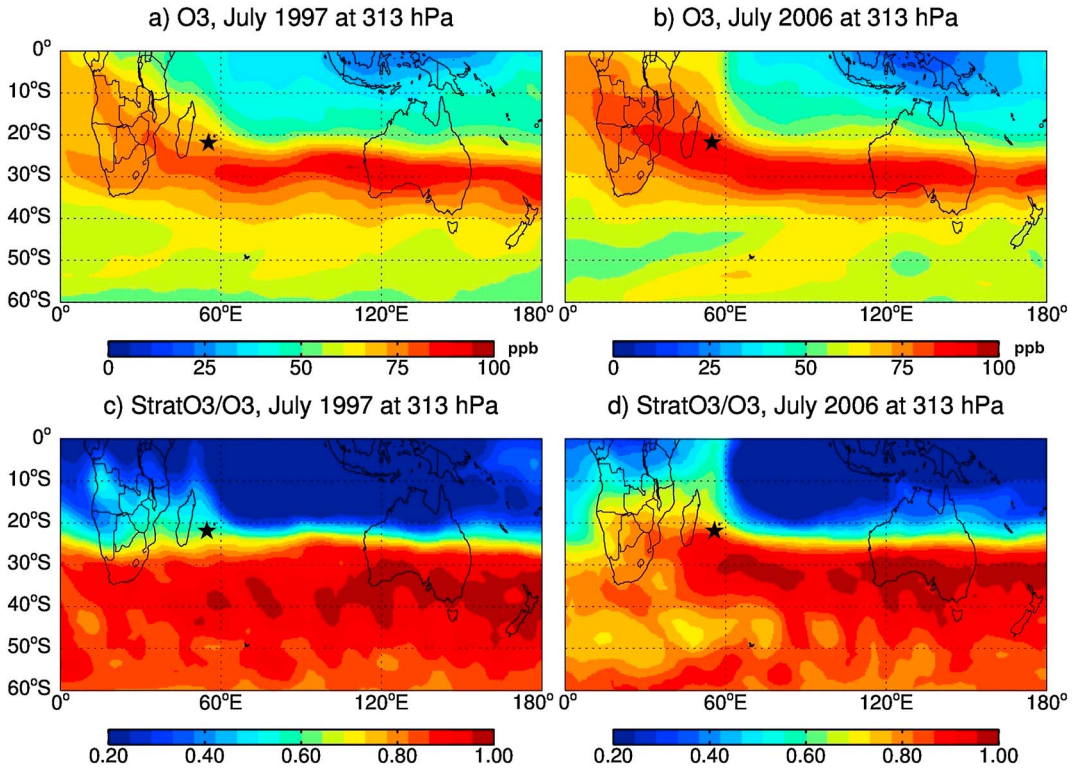

Figure 7. The monthly mean GMI-CTM Hindacast-VE simulated ozone mixing ratio at 313 hPa in (a) July 1997 and (b) July 2006 and the simulated monthly mean $Strat O_3/O_3$ ratio in (c) July 1997 and (d) July 2006. The black star denotes the Réunion Island.

(Figure 7). The combined contributions from horizontal and vertical dynamics result in the ozone maximum in 2006 at Réunion. The IAV of large-scale wind patterns reinforce the changes in the stratospheric contribution and contribute to IAV of upper tropospheric ozone.

3.3. Trends

Figure 10 shows the trend profiles as a function of month for the observations and model simulation (Hindcast-VE) at Réunion from 1992 to 2014 in units of ppb/decade. The trends are calculated from a linear

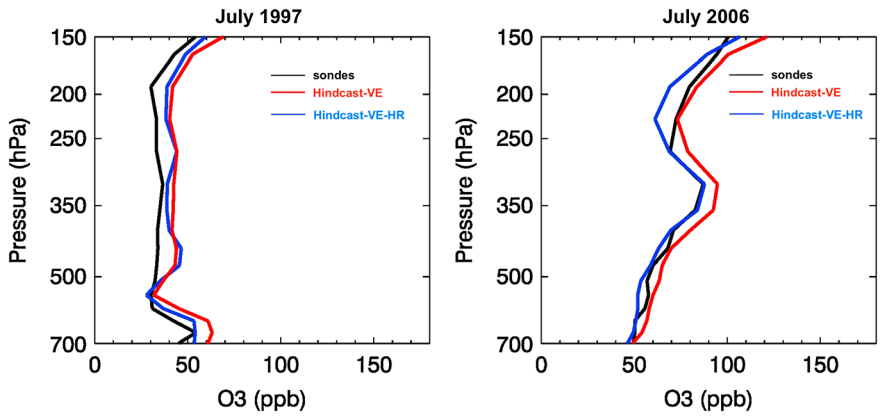

Figure 8. The profile of the monthly mean ozone in (left) July 1997 and (right) July 2006 from Réunion sonde observations (black), GMI-CTM Hindcast-VE (red), and GMI-CTM Hindcast-VE-HR simulations (blue). The model results are sampled on the date of sonde measurements.

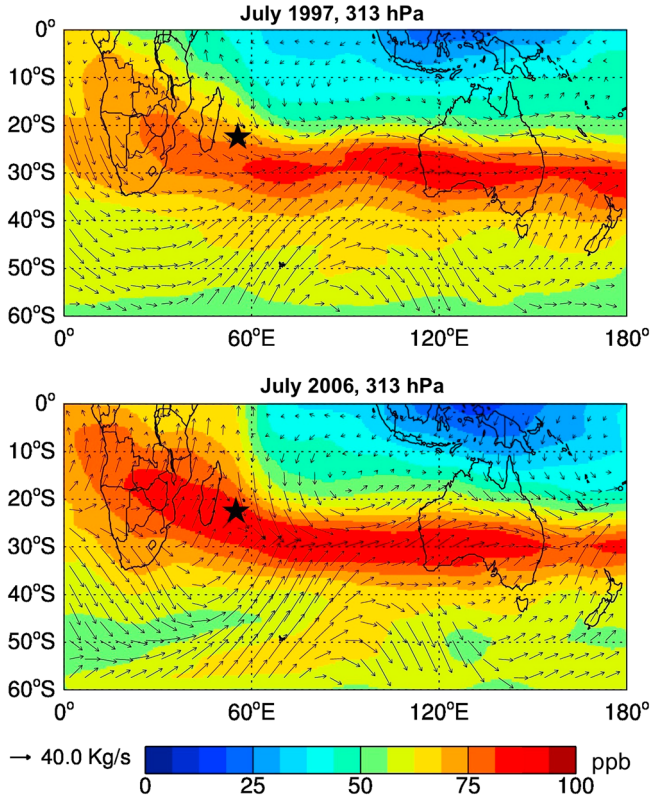

Figure 9. Monthly mean ozone mixing ratio (ppb) overlaid with horizontal winds derived from MERRA met fields in (top) July 1997 and (bottom) July 2006 at 313 hPa for the GMI Hindcast-VE simulation. The black star denotes the Réunion.

regression trend model that includes factors of the seasonal cycle and trends as discussed by *Ziemke et al.* [1997]. The black lines indicate statistical significance at 90% confidence interval. Similar profiles of trends calculated from the ozonesondes but for 1992–2011 (as in *Thompson et al.* [2014]) are shown in Figure S1 in the supporting information. The trend maximum in JJA in the middle and upper troposphere calculated for 1992–2014 is about 19 ppb/decade at 164 hPa (Figure 10a), which is ~5 ppb/decade lower than the trend maximum for 1992–2011, showing the sensitivity of the trend to the selected period. The model simulations reproduce the key features and general morphology of observed trends but underestimate the maximum trend in the sonde data in July–August in the middle and upper troposphere by ~6 ppb/decade (Hindcast-VE, Figure 10b). The model cosampled with the available sonde observations also shows statistically significant positive trends between 200 and 400 hPa in November–December, in agreement with the observed secondary maximum (Figure 10a).

3.4. Sensitivity to Time-Dependent Emissions

Figure 11 shows the temporal variation of total NO emissions and NO emissions from fossil fuel and biomass burning in our model in July–September from 1992 to 2011 over southern Africa and eastern regions. In southern Africa, the NO emissions are mainly driven by the IAV of biomass burning. Both fossil fuel and biomass burning emissions show a slightly positive trend in July–September. In the eastern region, the trend of NO emission is mainly driven by the fossil fuel combustions, and biomass burning contributes to the IAV. For example, the 1997 peak in NO emissions over the eastern region was driven by the record-setting forest fires in Indonesia. The fossil fuel emissions from the eastern region show a substantial increase over 20 years, which could contribute to the observed positive trends at Réunion through the pathway described earlier. We examined the effects of varied emission on tropospheric ozone over Réunion using a sensitivity run with constant emissions. Figure 12 shows the calculated ozone trend from 1992 to 2011, the period that the Hindcast-VE has the yearly varied emissions input, between

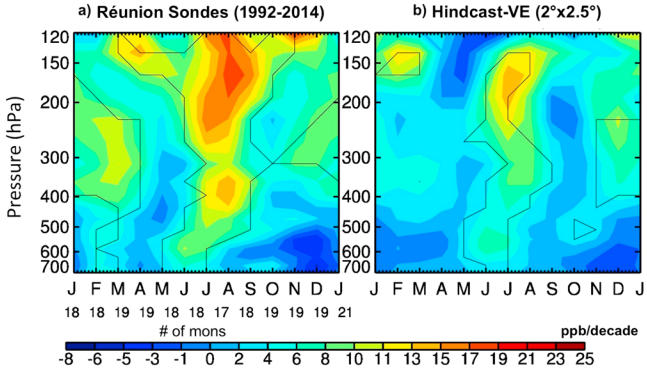

Figure 10. Trend (ppb/decade) computed from a linear regression model for ozone profile data from (a) Réunion sonde and (b) Hindcast-VE from 1992 to 2014. The model results are sampled on the date of sonde measurements. Black line contour denotes statistical significance at 90% confidence interval. "# of mons" at the bottom of Figure 10a shows the number of data points in the trend calculation for that month in our regression model.

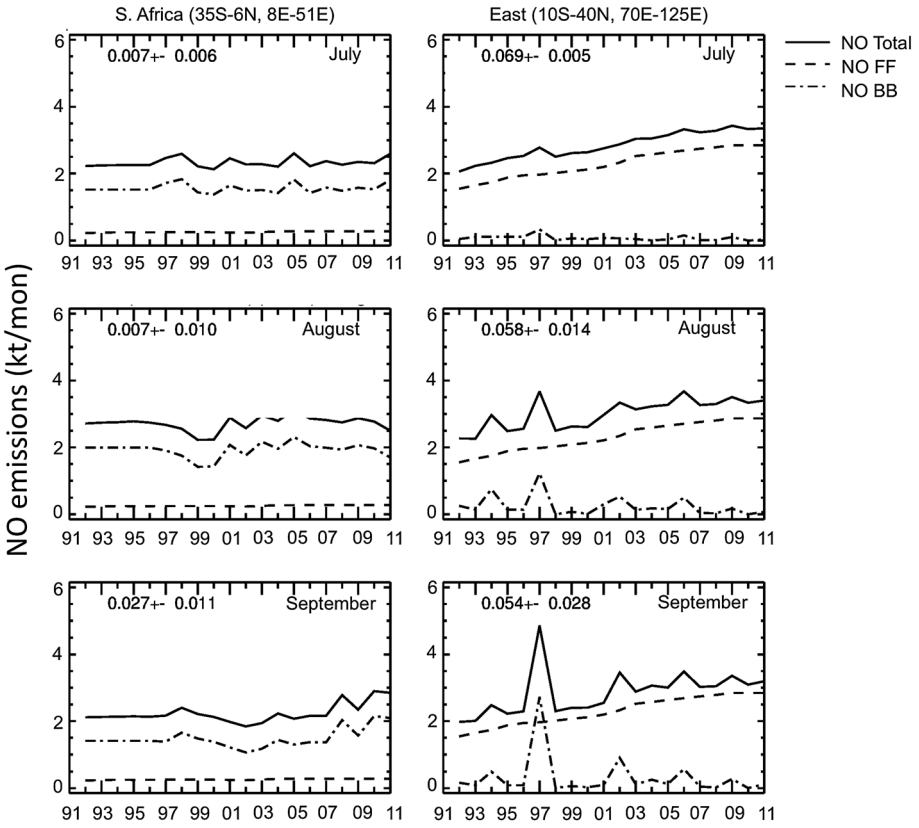

Figure 11. Temporal variation of emission of total NO (solid line), NO from fossil fuel (dash line), and NO from biomass burning (dash-dotted line) in our model in July–September from 1992 to 2011 over southern Africa and eastern regions. Numbers in each panel represent the calculated linear trends at the 90% confidence level with unit kt/month/yr.

runs with varied emission and constant emission (Hindcast-VE and Hindcast-CE). It shows that differences of simulated ozone trends between these two runs are quite small (<1 ppb/decade). The maximum increases due to emission changes occur in the upper troposphere from July to September and near the surface from August and September. The increase in the upper troposphere is probably caused by the cross-equator transport of increased emissions from the eastern region in the upper troposphere. The near-surface ozone increase in August–September possibly results from increased emissions over southern Africa and Madagascar. *Senten et al.* [2008] confirmed the impacts from burning events in Africa and Madagascar on the tropospheric chemical composition over Reunion based on an event study in October 2004, using the

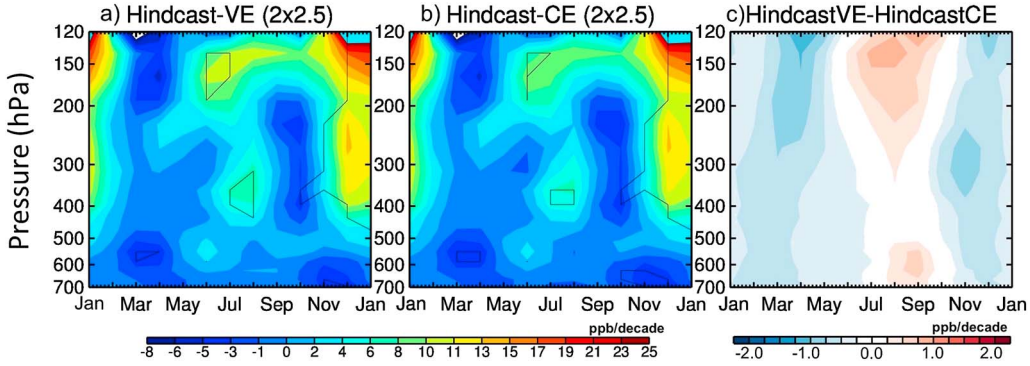

Figure 12. Trend (ppb/decade) computed from a linear regression model for monthly mean ozone profiles, calculated from daily profiles sampled at sonde time, from (a) Hindcast-VE and (b) Hindcast-CE from 1992 to 2011. (c) The difference of the trends between these two runs in unit ppb/decade.

measurements from ground-based high spectral resolution Fourier transform infrared solar absorption spectroscopy campaign and the FLEXPART ("FLEXible PARTicle dispersion model") simulation. The results in Figure 12 imply that the increase due to emission only accounts for ~15% of the ozone change and does not explain the observed trend maximum in the middle and upper troposphere over Réunion during austral winter.

4. Summary and Discussion

In this study we used the GMI-CTM model to interpret the trend and interannual variations of tropospheric ozone recorded by ozonesondes from 1991 to 2014 over Réunion. Comparisons of the observations and simulations, along with an analysis of the MERRA meteorology, the influence of surface emissions, and of stratospheric contributions using the $StratO_3$ tracer, provide an understanding of factors controlling the temporal variations of tropospheric ozone at this location. Our analysis also reveals limitations of low-resolution model simulations, as well as successes. It also implies that the bimonthly/monthly sonde measurements at Reunion are too sparse to give reliable trend estimates.

The model reproduces 61% of the observed interannual variance of tropospheric ozone over Réunion in July and less in August (27%) at 313 hPa. During the years with relatively low ozone, Réunion is mainly influenced by tropical marine air and the stratospheric influence is at a minimum. During the years with relatively high ozone, the stratospheric contribution reaches a maximum. The agreement between $StratO_3$, the model ozone, and observed ozone provides convincing evidence that the stratospheric influence plays an important role in controlling the IAV of tropospheric ozone over Réunion. Our examination of the horizontal wind pattern suggested that the IAV of large-scale wind patterns could be an important factor in the changes from the stratospheric contribution and also contribute to IAV of the ozone at 313 hPa. The simulated IAVs of tropospheric ozone between runs with interannually varying surface emissions and constant emissions are almost identical (not shown), indicating that the IAV in emissions does not contribute to the tropospheric ozone IAV over Réunion.

The GMI model cosampled with the available sonde observations captures the seasonality of trends implied by the Réunion ozonesondes, with positive trends during the July–September as well as during the December–January, notably in the middle and upper troposphere. However, the model simulation underestimates the magnitude of the maximum trend in sonde data in July–September. For the Hindcast-VE simulation, Réunion is located at the northernmost edge of the selected $2° \times 2.5°$ grid cell, which centers at 22°S, 55°E. The mean value of ozone in this grid cell would be larger than its northernmost edge value (21°S at Réunion) if the location of the large latitudinal gradient in ozone moves to the south. The overestimate decreases when Réunion falls in the high ozone region as the location with large latitudinal ozone gradient moves northward. Therefore, the changes in simulation errors due to coarse horizontal resolution could buffer the actual changes. The magnitude of ozone trends implied by the Réunion sondes is unlikely to be fully reproduced in the coarse-resolution 3-D model ($2° \times 2.5°$). Increasing the spatial resolution of the simulation leads to somewhat better agreement with the observed ozone mean mixing ratio, but the improvements vary year by year. To fully capture the magnitude of observed trends, a simulation with even higher resolution for both the horizontal and vertical grid, as well as an accurate representation of the vertical transport processes and of the location of the subtropical jet, may be needed. Our model analysis shows that the frequency of sondes at Reunion would have to be increased to at least weekly give reliable trends.

Many studies [e.g., *Pickering et al*., 1990; *Lelieveld and Dentener*, 2000] have shown that lightning NO_x is one of the important factors affecting tropospheric ozone in the tropics, especially at the middle and upper troposphere. In our hindcast simulation, lightning NO*x* are calculated online following the scheme described by *Allen et al*. [2010], showing spatial variations, but with a constant global total value every year. A recent study by *Murray et al*. [2013] compared the variance in the tropospheric ozone column for 1998–2006 between a simulation using IAV in lightning from Lightning Imaging Sensor and a base simulation with IAV only from GEOS convection. Their results show that the difference is exceedingly small at Réunion. We conclude that the lightning NO_x scheme in our hindcast simulation is not the reason for not fully capturing the observed ozone variability over Réunion.

The emission influence on the trends or IAV of tropospheric O_3 reflects remote effects from emission sources through long-range transport. Increased emissions over the eastern region contribute partially to the ozone

increase in the upper troposphere in austral winter. Increasing emissions over southern Africa appear to affect only the lower troposphere and do not explain the observed trend maximum in the middle and upper troposphere during its austral winter season.

A recent model study by *Li et al*. [2010] based on simulations from a coupled chemistry-climate model (GEOSCCM) has identified a narrowing of the Hadley cell's rising branch with enhanced descent extending into the tropics over the 21st century (2001–2099). Their simulations suggested that the expansion of the sinking branches of the Hadley cell occurred on both the equatorward and poleward edges. The expansion of poleward edges is commonly referred to as a widening of the tropical belt in various observational and modeling studies [e.g., *Hu and Fu*, 2007; *Seidel and Randel*, 2007]. The expansion of equatorward edges is associated with an equatorward movement and leads to the narrowing of the Hadley cell's rising branch, which is likely to produce an increased stratospheric input over Réunion Island and result in increased tropospheric ozone near this region. Weekly ozonesonde measurements at this location will be promising for understanding the long-term variations in dynamical exchanges between the tropics and midlatitudes and between the troposphere and the stratosphere due to its special location. It will also be valuable for evaluations of climate predictions from a chemistry-climate model.

Acknowledgments

All model output used for this article can be obtained by contacting J. Liu (e-mail: Junhua.liu@nasa.gov). I gratefully acknowledge the financial support by NASA's Atmospheric Chemistry Modeling and Analysis Program (ACMAP) (grant NNH12ZDA001N). Work was performed under contract with NASA at Goddard. The sonde program at Réunion was initiated in 1991/1992 with the support of the CNRS and the University of La Réunion; after 1997, additional funding came from SHADOZ through the Upper Atmosphere Research Program of NASA (thanks to M.J. Kurylo and K.W. Jucks) with contributions from NOAA/GMD and NASA's Aura Validation. Thanks to J.L. Baray (the LaMP/OPGC, FRANCE) for sonde data from September 1992 to December 1997. Sonde data after 1998 can be obtained from SHADOZ website (http://croc.gsfc.nasa.gov/shadoz/). Thanks to J.M. Metzger (University of La Réunion) for the ongoing technical support of the sounding program. I would like to thank S. Pawson and K. Wargan for their helpful discussion on GMAO assimilated ozone products. I benefited from useful discussions with J. Ziemke.

References

Allen, D., K. Pickering, B. Duncan, and M. Damon (2010), Impact of lightning NO emissions on North American photochemistry as determined using the Global Modeling Initiative (GMI) model, *J. Geophys. Res.*, *115*, D22301, doi:10.1029/2010JD014062.

Baldy, S., G. Ancellet, M. Bessafi, A. Badr, and D. L. S. Luk (1996), Field observations of the vertical distribution of tropospheric ozone at the island of Reunion (southern tropics), *J. Geophys. Res.*, *101*(D19), 23,835–23,849, doi:10.1029/95JD02929.

Baray, J. L., G. Ancellet, F. G. Taupin, M. Bessafi, S. Baldy, and P. Keckhut (1998), Subtropical tropopause break as a possible stratospheric source of ozone in the tropical troposphere, *J. Atmos. Sol. Terr. Phys.*, *60*(1), 27–36, doi:10.1016/s1364-6826(97)00116-8.

Baray, J. L., S. Baldy, R. D. Diab, and J. P. Cammas (2003), Dynamical study of a tropical cut-off low over South Africa, and its impact on tropospheric ozone, *Atmos. Environ.*, *37*(11), 1475–1488, doi:10.1016/s1352-2310(02000999-8.

Baray, J. L., et al. (2006), An instrumented station for the survey of ozone and climate change in the southern tropics, *J. Environ. Monit.*, *8*(10), 1020–1028, doi:10.1039/b607762e.

Bell, M. L., F. Dominici, and J. M. Samet (2005), A meta-analysis of time-series studies of ozone and mortality with comparison to the national morbidity, mortality, and air pollution study, *Epidemiology*, *16*(4), 436–445, doi:10.1097/01.ede.0000165817.40152.85.

Brewer, A. W. (1949), Evidence for a world circulation provided by the measurements of helium and water vapour distribution in the stratosphere, *Q. J. R. Meteorol. Soc.*, *75*(326), 351–363, doi:10.1002/qj.49707532603.

Chin, M., P. Ginoux, S. Kinne, O. Torres, B. N. Holben, B. N. Duncan, R. V. Martin, J. A. Logan, A. Higurashi, and T. Nakajima (2002), Tropospheric aerosol optical thickness from the GOCART model and comparisons with satellite and Sun photometer measurements, *J. Atmos. Sci.*, *59*(3), 461–483.

Clain, G., J. L. Baray, R. Delmas, R. Diab, J. L. de Bellevue, P. Keckhut, F. Posny, J. M. Metzger, and J. P. Cammas (2009), Tropospheric ozone climatology at two Southern Hemisphere tropical/subtropical sites, (Reunion Island and Irene, South Africa) from ozonesondes, LIDAR, and in situ aircraft measurements, *Atmos. Chem. Phys.*, *9*(5), 1723–1734.

Cooper, O. R., et al. (2010), Increasing springtime ozone mixing ratios in the free troposphere over western North America, *Nature*, *463*(7279), 344–348, doi:10.1038/nature08708.

De Bellevue, J. L., J. L. Baray, S. Baldy, G. Ancellet, R. Diab, and F. Ravetta (2007), Simulations of stratospheric to tropospheric transport during the tropical cyclone Marlene event, *Atmos. Environ.*, *41*(31), 6510–6526, doi:10.1016/j.atmosenv.2007.04.040.

Dobson, G. M. B. (1956), Origin and distribution of the polyatomic molecules in the atmosphere, *Proc. R. Soc. London, Ser. A*, *236*(1205), 187–193, doi:10.1098/rspa.1956.0127.

Duncan, B. N., R. V. Martin, A. C. Staudt, R. Yevich, and J. A. Logan (2003), Interannual and seasonal variability of biomass burning emissions constrained by satellite observations, *J. Geophys. Res.*, *108*(D2), 4100, doi:10.1029/2002JD002378.

Duncan, B. N., S. E. Strahan, Y. Yoshida, S. D. Steenrod, and N. Livesey (2007), Model study of the cross-tropopause transport of biomass burning pollution, *Atmos. Chem. Phys.*, *7*(14), 3713–3736.

Fiore, A. M., D. J. Jacob, B. D. Field, D. G. Streets, S. D. Fernandes, and C. Jang (2002), Linking ozone pollution and climate change: The case for controlling methane, *Geophys. Res. Lett.*, *29*(19), 1919, doi:10.1029/2002GL015601.

Forster, P. M., G. Bodeker, R. Schofield, S. Solomon, and D. Thompson (2007), Effects of ozone cooling in the tropical lower stratosphere and upper troposphere, *Geophys. Res. Lett.*, *34*, L23813, doi:10.1029/2007GL031994.

Fusco, A. C., and J. A. Logan (2003), Analysis of 1970–1995 trends in tropospheric ozone at Northern Hemisphere midlatitudes with the GEOS-CHEM model, *J. Geophys. Res.*, *108*(D15), 4449, doi:10.1029/2002JD002742.

Garstang, M., P. D. Tyson, R. Swap, M. Edwards, P. Kallberg, and J. A. Lindesay (1996), Horizontal and vertical transport of air over southern Africa, *J. Geophys. Res.*, *101*(D19), 23,721–23,736, doi:10.1029/95JD00844.

Guenther, A., T. Karl, P. Harley, C. Wiedinmyer, P. I. Palmer, and C. Geron (2006), Estimates of global terrestrial isoprene emissions using MEGAN (Model of Emissions of Gases and Aerosols from Nature), *Atmos. Chem. Phys.*, *6*, 3181–3210.

Hastenrath, S., and M. C. Wu (1982), Oscillations of upper-air circulation and anomalies in the surface climate of the tropics, *Arch. Meteorol., Geophys. Bioklimatol., Ser. B*, *31*(1–2), 1–37, doi:10.1007/bf02311340.

Hess, P. G., and R. Zbinden (2013), Stratospheric impact on tropospheric ozone variability and trends: 1990–2009, *Atmos. Chem. Phys.*, *13*(2), 649–674, doi:10.5194/acp-13-649-2013.

Hess, P. G., D. Kinnison, and Q. Tang (2015), Ensemble simulations of the role of the stratosphere in the attribution of tropospheric ozone variability, *Atmos. Chem. Phys.*, *15*, 2341–2365, doi:10.5194/acp-2315-2341-2015.

Holton, J. R., P. H. Haynes, M. E. McIntyre, A. R. Douglass, R. B. Rood, and L. Pfister (1995), Stratosphere-troposphere exchange, *Rev. Geophys.*, *33*(4), 403–439, doi:10.1029/95RG02097.

Hoskins, B. J., and M. J. Rodwell (1995), A model of the Asian summer monsoon: 1. The global-scale, *J. Atmos. Sci.*, *52*(9), 1329–1340, doi:10.1175/1520-0469(1995)052<1329:amotas>2.0.co;2.
Hu, Y., and Q. Fu (2007), Observed poleward expansion of the Hadley circulation since 1979, *Atmos. Chem. Phys.*, *7*(19), 5229–5236.
Karlsdottir, S., I. S. A. Isaksen, G. Myhre, and T. K. Berntsen (2000), Trend analysis of O_3 and CO in the period 1980–1996: A three-dimensional model study, *J. Geophys. Res.*, *105*(D23), 28,907–28,933, doi:10.1029/2000JD900374.
Lacis, A. A., D. J. Wuebbles, and J. A. Logan (1990), Radiative forcing of climate by changes in the vertical distribution of ozone, *J. Geophys. Res.*, *95*(D7), 9971–9981, doi:10.1029/JD095iD07p09971.
Lelieveld, J., and F. J. Dentener (2000), What controls tropospheric ozone?, *J. Geophys. Res.*, *105*(D3), 3531–3551, doi:10.1029/1999JD901011.
Lelieveld, J., J. van Aardenne, H. Fischer, M. de Reus, J. Williams, and P. Winkler (2004), Increasing ozone over the Atlantic Ocean, *Science*, *304*(5676), 1483–1487, doi:10.1126/science.1096777.
Li, F., R. S. Stolarski, S. Pawson, P. A. Newman, and D. Waugh (2010), Narrowing of the upwelling branch of the Brewer-Dobson circulation and Hadley cell in chemistry-climate model simulations of the 21st century, *Geophys. Res. Lett.*, *37*, L13702, doi:10.1029/2010GL043718.
Lin, M., A. M. Fiore, O. R. Cooper, L. W. Horowitz, A. O. Langford, H. Levy II, B. J. Johnson, V. Vaishali Naik, S. J. Oltmans, and C. J. Senff (2012), Springtime high surface ozone events over the western United States: Quantifying the role of stratospheric intrusions, *J. Geophys. Res.*, *117*, D00V22, doi:10.1029/2012JD018151.
Lin, M., L. W. Horowitz, S. J. Oltmans, A. M. Fiore, and S. Fan (2014), Tropospheric ozone trends at Mauna Loa Observatory tied to decadal climate variability, *Nat. Geosci.*, *7*(2), 136–143, doi:10.1038/ngeo2066.
Lin, M., A. M. Fiore, L. W. Horowitz, A. O. Langford, S. J. Oltmans, D. Tarasick, and H. E. Rieder (2015), Climate variability modulates western US ozone air quality in spring via deep stratospheric intrusions, *Nat. Commun.*, *6*, doi:10.1038/ncomms8105.
Logan, J. A. (1999), An analysis of ozonesonde data for the troposphere: Recommendations for testing 3-D models and development of a gridded climatology for tropospheric ozone, *J. Geophys. Res.*, *104*(D13), 16,115–16,149, doi:10.1029/1998JD100096.
Logan, J. A., and V. Kirchhoff (1986), Seasonal variations of tropospheric ozone at natal, brazil, *J. Geophys. Res.*, *91*(D7), 7875–7881, doi:10.1029/JD091iD07p07875.
Logan, J. A., M. J. Prather, S. C. Wofsy, and M. B. McElroy (1981), Tropospheric chemistry: A global perspective, *J. Geophys. Res.*, *86*(NC8), 7210–7254, doi:10.1029/JC086iC08p07210.
Logan, J. A., I. Megretskaia, R. Nassar, L. T. Murray, L. Zhang, K. W. Bowman, H. M. Worden, and M. Luo (2008), Effects of the 2006 El Nino on tropospheric composition as revealed by data from the Tropospheric Emission Spectrometer (TES), *Geophys. Res. Lett.*, *35*, L03816, doi:10.1029/2007GL031698.
Logan, J. A., et al. (2012), Changes in ozone over Europe: Analysis of ozone measurements from sondes, regular aircraft (MOZAIC) and alpine surface sites, *J. Geophys. Res.*, *117*, D09301, doi:10.1029/2011JD016952.
McLinden, C. A., S. C. Olsen, B. Hannegan, O. Wild, M. J. Prather, and J. Sundet (2000), Stratospheric ozone in 3-D models: A simple chemistry and the cross-tropopause flux, *J. Geophys. Res.*, *105*(D11), 14,653–14,665, doi:10.1029/2000JD900124.
Moorthi, S., and M. J. Suarez (1992), Relaxed Arakawa-Schubert—A parameterization of moist convection for general circulation models, *Mon. Weather Rev.*, *120*(6), 978–1002, doi:10.1175/1520-0493(1992)120<0978:rasapo>2.0.co;2.
Murray, L. T., J. A. Logan, and D. J. Jacob (2013), Interannual variability in tropical tropospheric ozone and OH: The role of lightning, *J. Geophys. Res. Atmos.*, *118*, 11,468–11,480, doi:10.1002/jgrd.50857.
Olivier, J. G. J., J. A. Van Aardenne, F. J. Dentener, V. Pagliari, L. N. Ganzeveld, and J. A. H. W. Peters (2005), Recent trends in global greenhouse gas emissions: Regional trends and spatial distribution of key sources, in *Non-CO_2 Greenhouse Gases (NCGG-4)*, coordinator: van Amstel, A., pp. 325–330, Millpress, Rotterdam.
Pickering, K. E., A. M. Thompson, R. R. Dickerson, W. T. Luke, D. P. McNamara, J. P. Greenberg, and P. R. Zimmerman (1990), Model calculations of tropospheric ozone production potential following observed convective events, *J. Geophys. Res.*, *95*(D9), 14,049–14,062, doi:10.1029/JD095iD09p14049.
Piketh, S. J., R. J. Swap, W. Maenhaut, H. J. Annegam, and P. Formenti (2002), Chemical evidence of long-range atmospheric transport over southern Africa, *J. Geophys. Res.*, *107*(D24), 4817, doi:10.1029/2002JD002056.
Postel, G. A., and M. H. Hitchman (1999), A climatology of Rossby wave breaking along the subtropical tropopause, *J. Atmos. Sci.*, *56*(3), 359–373, doi:10.1175/1520-0469(1999)056<0359:acorwb>2.0.co;2.
Pozzoli, L., G. Janssens-Maenhout, T. Diehl, I. Bey, M. G. Schultz, J. Feichter, E. Vignati, and F. Dentener (2011), Re-analysis of tropospheric sulfate aerosol and ozone for the period 1980–2005 using the aerosol-chemistry-climate model ECHAM5-HAMMOZ, *Atmos. Chem. Phys.*, *11*(18), 9563–9594, doi:10.5194/acp-11-9563-2011.
Prather, M. J., X. Zhu, Q. Tang, J. N. Hsu, and J. L. Neu (2011), An atmospheric chemist in search of the tropopause, *J. Geophys. Res.*, *116*, D04306, doi:10.1029/2010JD014939.
Randriambelo, T., J. L. Baray, and S. Baldy (2000), Effect of biomass burning, convective venting, and transport on tropospheric ozone over the Indian Ocean: Reunion Island field observations, *J. Geophys. Res.*, *105*(D9), 11,813–11,832, doi:10.1029/1999JD901097.
Randriambelo, T., J. L. Baray, S. Baldy, A. M. Thompson, S. Oltmans, and P. Keckhut (2003), Investigation of the short-time variability of tropical tropospheric ozone, *Ann. Geophys.*, *21*(10), 2095–2106.
Rienecker, M. M., et al. (2011), MERRA: NASA's Modern-Era Retrospective Analysis for Research and Applications, *J. Clim.*, *24*(14), 3624–3648, doi:10.1175/jcli-d-11-00015.1.
Rodwell, M. J., and B. J. Hoskins (2001), Subtropical anticyclones and summer monsoons, *J. Clim.*, *14*(15), 3192–3211, doi:10.1175/1520-0442(2001)014<3192:saasm>2.0.co;2.
Saunois, M., L. Emmons, J. F. Lamarque, S. Tilmes, C. Wespes, V. Thouret, and M. Schultz (2012), Impact of sampling frequency in the analysis of tropospheric ozone observations, *Atmos. Chem. Phys.*, *12*(15), 6757–6773, doi:10.5194/acp-12-6757-2012.
Sauvage, B., V. Thouret, A. M. Thompson, J. C. Witte, J. P. Cammas, P. Nedelec, and G. Athier (2006), Enhanced view of the "tropical Atlantic ozone paradox" and "zonal wave one" from the in situ MOZAIC and SHADOZ data, *J. Geophys. Res.*, *111*, D01301, doi:10.1029/2005JD006241.
Sauvage, B., R. V. Martin, A. van Donkelaar, and J. R. Ziemke (2007), Quantification of the factors controlling tropical tropospheric ozone and the South Atlantic maximum, *J. Geophys. Res.*, *112*, D11309, doi:10.1029/2006JD008008.
Seidel, D. J., and W. J. Randel (2007), Recent widening of the tropical belt: Evidence from tropopause observations, *J. Geophys. Res.*, *112*, D20113, doi:10.1029/2007JD008861.
Senten, C., et al. (2008), Technical note: New ground-based FTIR measurements at Ile de La Reunion—Observations, error analysis, and comparisons with independent data, *Atmos. Chem. Phys.*, *8*(13), 3483–3508.
Silva, R. A., et al. (2013), Global premature mortality due to anthropogenic outdoor air pollution and the contribution of past climate change, *Environ. Res. Lett.*, *8*(3), doi:10.1088/1748-9326/8/3/034005.

Sitch, S., P. M. Cox, W. J. Collins, and C. Huntingford (2007), Indirect radiative forcing of climate change through ozone effects on the land-carbon sink, *Nature*, *448*(7155), 791–U794, doi:10.1038/nature06059.

Skerlak, B., M. Sprenger, and H. Wernli (2014), A global climatology of stratosphere-troposphere exchange using the ERA-Interim data set from 1979 to 2011, *Atmos. Chem. Phys.*, *14*(2), 913–937, doi:10.5194/acp-14-913-2014.

Stevenson, D. S., et al. (2013), Tropospheric ozone changes, radiative forcing and attribution to emissions in the Atmospheric Chemistry and Climate Model Intercomparison Project (ACCMIP), *Atmos. Chem. Phys.*, *13*(6), 3063–3085, doi:10.5194/acp-13-3063-2013.

Stolarski, R. S., A. R. Douglass, S. Steenrod, and S. Pawson (2006), Trends in stratospheric ozone: Lessons learned from a 3D chemical transport model, *J. Atmos. Sci.*, *63*(3), 1028–1041.

Strahan, S. E., B. N. Duncan, and P. Hoor (2007), Observationally derived transport diagnostics for the lowermost stratosphere and their application to the GMI chemistry and transport model, *Atmos. Chem. Phys.*, *7*(9), 2435–2445.

Strode, S. A., J. M. Rodriguez, J. A. Logan, O. R. Cooper, J. C. Witte, L. N. Lamsal, M. Damon, B. Van Aartsen, S. D. Steenrod, and S. E. Strahan (2015), Trends and variability in surface ozone over the United States, *J. Geophys. Res. Atmos.*, *120*, 9020–9042, doi:10.1002/2014JD022784.

Sudo, K., and H. Akimoto (2007), Global source attribution of tropospheric ozone: Long-range transport from various source regions, *J. Geophys. Res.*, *112*, D12302, doi:10.1029/2006JD007992.

Taupin, F. G., M. Bessafi, S. Baldy, and P. J. Bremaud (1999), Tropospheric ozone above the southwestern Indian Ocean is strongly linked to dynamical conditions prevailing in the tropics, *J. Geophys. Res.*, *104*(D7), 8057–8066, doi:10.1029/98JD02456.

Thompson, A. M., K. E. Pickering, D. P. McNamara, M. R. Schoeberl, R. D. Hudson, J. H. Kim, E. V. Browell, V. Kirchhoff, and D. Nganga (1996), Where did tropospheric ozone over southern Africa and the tropical Atlantic come from in October 1992? Insights from TOMS, GTE TRACE A, and SAFARI 1992, *J. Geophys. Res.*, *101*(D19), 24,251–24,278, doi:10.1029/96JD01463.

Thompson, A. M., et al. (2003), Southern Hemisphere Additional Ozonesondes (SHADOZ) 1998–2000 tropical ozone climatology: 1. Comparison with Total Ozone Mapping Spectrometer (TOMS) and ground-based measurements, *J. Geophys. Res.*, *108*(D2), 8238, doi:10.1029/2001JD000967.

Thompson, A. M., J. C. Witte, H. G. J. Smit, S. J. Oltmans, B. J. Johnson, V. W. J. H. Kirchhoff, and F. J. Schmidlin (2007), Southern Hemisphere Additional Ozonesondes (SHADOZ) 1998–2004 tropical ozone climatology: 3. Instrumentation, station-to-station variability, and evaluation with simulated flight profiles, *J. Geophys. Res.*, *112*, D03304, doi:10.1029/2005JD007042.

Thompson, A. M., et al. (2012), Southern Hemisphere Additional Ozonesondes (SHADOZ) ozone climatology (2005–2009): Tropospheric and tropical tropopause layer (TTL) profiles with comparisons to OMI-based ozone products, *J. Geophys. Res.*, *117*, D23301, doi:10.1029/2011JD016911.

Thompson, A. M., N. V. Balashov, J. C. Witte, J. G. R. Coetzee, V. Thouret, and F. Posny (2014), Tropospheric ozone increases over the southern Africa region: Bellwether for rapid growth in Southern Hemisphere pollution?, *Atmos. Chem. Phys.*, *14*(18), 9855–9869, doi:10.5194/acp-14-9855-2014.

van der Werf, G. R., J. T. Randerson, L. Giglio, G. L. Collatz, M. Mu, P. S. Kasibhatla, D. C. Morton, R. S. DeFries, Y. Jin, and T. T. van Leeuwen (2010), Global fire emissions and the contribution of deforestation, savanna, forest, agricultural, and peat fires (1997–2009), *Atmos. Chem. Phys.*, *10*, 16,153–16,230.

Wargan, K., S. Pawson, M. A. Olsen, J. C. Witte, A. R. Douglass, J. R. Ziemke, S. E. Strahan, and J. E. Nielsen (2015), The global structure of upper troposphere-lower stratosphere ozone in GEOS-5: A multiyear assimilation of EOS Aura data, *J. Geophys. Res. Atmos.*, *120*, 2013–2036, doi:10.1002/2014JD022493.

Waugh, D. W., and L. M. Polvani (2000), Climatology of intrusions into the tropical upper troposphere, *Geophys. Res. Lett.*, *27*(23), 3857–3860, doi:10.1029/2000GL012250.

Ziemke, J. R., S. Chandra, R. D. McPeters, and P. A. Newman (1997), Dynamical proxies of column ozone with applications to global trend models, *J. Geophys. Res.*, *102*(D5), 6117–6129, doi:10.1029/96JD03783.

Ziemke, J. R., S. Chandra, and P. K. Bhartia (2001), "Cloud slicing": A new technique to derive upper tropospheric ozone from satellite measurements, *J. Geophys. Res.*, *106*(D9), 9853–9867, doi:10.1029/2000JD900768.

Ziemke, J. R., et al. (2014), Assessment and applications of NASA ozone data products derived from Aura OMI/MLS satellite measurements in context of the GMI chemical transport model, *J. Geophys. Res. Atmos.*, *119*, 5671–5699, doi:10.1002/2013JD020914.